Journal of Hazardous Materials 387 (2020) 122001

Contents lists available at ScienceDirect

Journal of Hazardous Materials

journal homepage: www.elsevier.com/locate/jhazmat

Sensitivity programmable ratiometric electrochemical aptasensor based on signal engineering for the detection of aflatoxin B1 in peanut

Yuye Li[a], Dong Liu[a,*], Chengxi Zhu[a], Xiuli Shen[a], Yang Liu[b], Tianyan You[a,*]

[a] Key Laboratory of Modern Agricultural Equipment and Technology, Ministry of Education, School of Agricultural Equipment Engineering, Jiangsu University, Zhenjiang, Jiangsu 212013, China

[b] College of Science and Engineering, James Cook University, Townsville, Queensland 4811, Australia

GRAPHICAL ABSTRACT

A sensitivity programmable ratiometric electrochemical aptasensor was fabricated based on thionine-graphene nanocomposite for the detection of AFB1 in peanut.

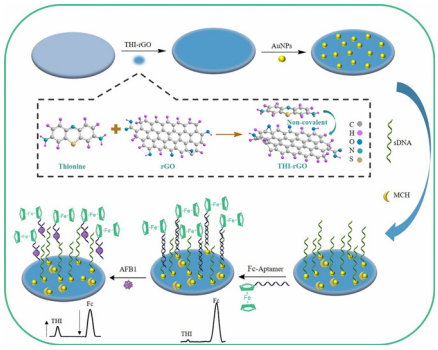

ARTICLE INFO

Editor: R. Teresa

Keywords:
Hazardous materials
Aflatoxin B1
Ratiometric electrochemical aptasensor
Programmable sensitivity

ABSTRACT

Accurately monitoring of aflatoxin B1 (AFB1), the most hazardous mycotoxin in agricultural products, is essential for the public health, but various testing demands (e.g. detection range, sensitivity) for different samples can be challenging for sensors. Here, we developed a sensitivity-programmable ratiometric electrochemical aptasensor for AFB1 analysis in peanut. Thionine functionalized reduced graphene oxide (THI-rGO) served as reference signal generator, ferrocene-labelled aptamer (Fc-apt) output the response signal. During analysis, the formation of Fc-apt-AFB1 complex led to its stripping from the electrode and faded the current intensity of Fc (I_{Fc}), while the current intensity of THI (I_{THI}) was enhanced. And ratiometric detection of AFB1 was achieved by using the current intensity ratio (I_{THI}/I_{Fc}) as quantitative signal. Compared with ratiometric strategies that highly rely on the labelled aptamers, the proposed strategy could regulate the value of I_{THI}/I_{Fc} by changing the modification of Fc-apt. And the detection sensitivity was found to be closely related to I_{THI}/I_{Fc}. Under the optimal conditions, the fabricated aptasensor with a dynamic range from 0.05–20 ng mL^{-1} and a detection limit of 0.016 ng mL^{-1} for AFB1 analysis. Besides, it exhibited excellent selectivity, reliability and reproducibility. The proposed sensitivity-programmable biosensor can be applied to detect various aptamer-recognized mycotoxins in agricultural sensing.

* Corresponding author.
E-mail addresses: dongliu@ujs.edu.cn (D. Liu), youty@ujs.edu.cn (T. You).

https://doi.org/10.1016/j.jhazmat.2019.122001
Received 9 October 2019; Received in revised form 11 December 2019; Accepted 29 December 2019
Available online 30 December 2019

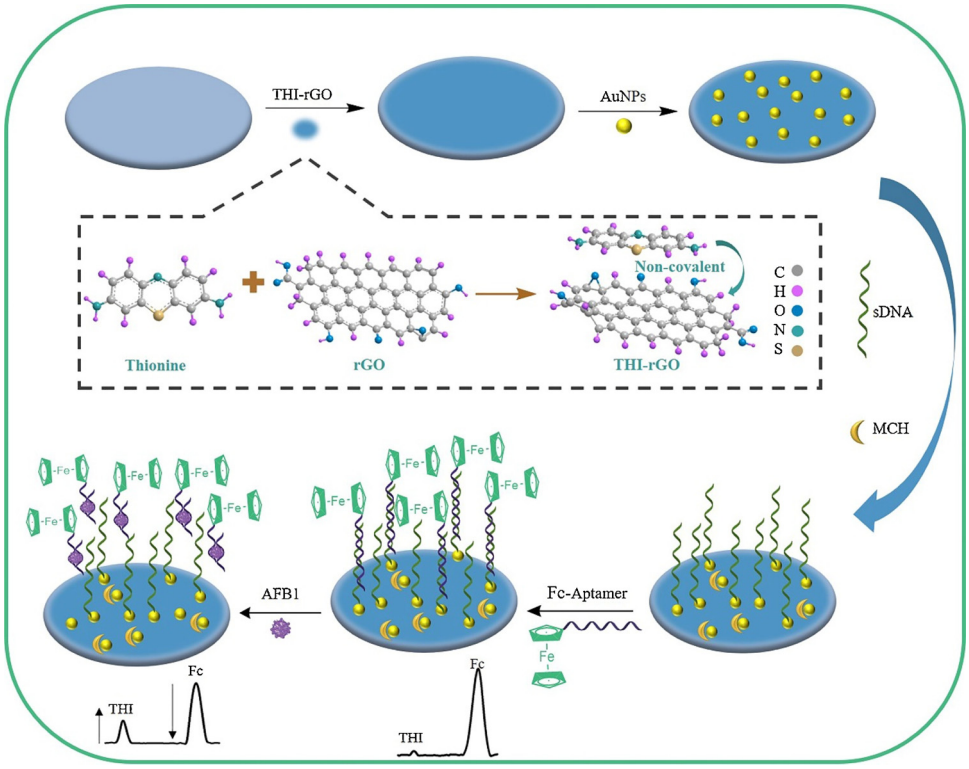

Scheme 1. Schematic illustration of the fabrication of the AFB1 aptasensor.

1. Introduction

Aflatoxins, produced by aspergillus parasiticus and aspergillus flavus, are a category of extreme hazardous metabolites and emerge to be the inevitable contaminant in food and feedstuffs (e.g. peanut, corn) (Crisan, 1973; Daradimos et al., 2000; Zhuang et al., 2016; Karapetis et al., 2018). As the most toxic specie, aflatoxin B1 (AFB1) has been identified as the first carcinogen by the Agency for Research on Cancer (IARC) (WHO, 1993). And it has posed a world-widely threat to the public health, e.g. the incidence rate of AFB1 in feed ingredients and feed samples reaches up to 33.9 % in central China (Liu et al., 2016). For the sake of food safety, many countries have a maximum allowable limit for AFB1 in agricultural products, food and feeds, e.g. $10-50\,\mu g\,kg^{-1}$ in grain by China (GB13078.2–2006) and $5-20\,\mu g\,kg^{-1}$ by European Union, while the content in human food ranged from $0.05\,\mu g\,kg^{-1}$ in European Union to $20\,\mu g\,kg^{-1}$ in United States (Babu and Muriana, 2011).

State-of-the-art methods including high-performance liquid chromatography-mass spectrometry (HPLC-MS), thin-layer chromatography (TLC) and LC combined with mass spectrometry (MS) have been widely used to monitor AFB1 pollution in lab but failed in terms of rapid and in-field testing. (Capriotti et al., 2014; Ko et al., 2015a; Ediage et al., 2011). For the lateral, the newly-emerging ratiometric electrochemical method, featuring comparable sensitivity, fast response, and ease-of-use, can be one of the promising alternatives. Such an assay is assumed to be capable of conquering the accidental errors and environmental influences by built-in correction with a dual-signal output mode, allowing the superior analytical reliability and accuracy (Yang et al., 2018). For the fabrication of sensors, current investigations mainly employ the target-induced conformational change of terminal redox-tagged DNA to output ratiometric signal that the response depends on the distance change of the redox tag and the electrode surface (Zhu et al., 2019). In terms of AFB1, to this end, at least one aptasensor has been proposed for AFB1 analysis, presenting the reduced signal fluctuation, enhanced sensitivity and higher value compared with that based on the single-signal mode (Wu et al., 2017).

Despite the attracting properties, the development of ratiometric electrochemical aptasensor faces a potential challenge: programming of dynamic range and sensitivity which may be essential for the smart sensing platform (Wang et al., 2017). Realistic demands of analytical properties for sensors can be various, e.g. wide dynamic range is required for viral load monitoring, and high sensitivity may be essential for drug monitoring (Goodman, 1996). For single signal-based sensors, these parameters can be tuned by the environmental changes or material size regulation to output a responsive signal (Jeong et al., 2017; Zhang et al., 2014; Shimizu et al., 2017). However, such strategies may be unusable for classic ratiometric electrochemical aptasensors with the instinct to overcome these interferes. Generally, investigation is rarely focused on the regulation of ratiometric signal owing to the following reasons: 1) Various relationships between the current intensity and distance for different redox tags (Li et al., 2019). Such phenomenon has been observed in the sensors fabricated with ferrocene (Fc) and methylene blue (MB), which should significantly complicate the change of ratiometric signal by tag selection (Kékedy-Nagy and Ferapontova, 2018). 2) Influence of modification of redox tag on the affinity of DNA and signal intensity. Increasing the number of tags on DNA could be worked for ratiometric signal adjustment, however, anchoring sites are limited at DNA and it may affect the affinity between DNA and the target (Amaya-González et al., 2015). 3) Difficulty in the accurate and reproducible assembly of DNA on the electrode surface. Eliminating clustering, aggregation and nonspecific interactions of DNA remains challenging during the assembly of aptasensor, and these issues should render it extremely difficult to regulate the distance and in turn the signal (Bizzotto et al., 2018). Based on the above analysis, we can conclude that it would be extremely attracting, if we develop a ratiometric electrochemical aptasensor with programmable sensitivity.

Inspired by this, we proposed a ratiometric electrochemical aptasensor with the adjustable sensitivity for AFB1 analysis via the regulation of ratiometric signal. The detailed content is illustrated in Scheme 1. Thionine (THI) is a redox probe with good electrochemical

reversibility, stability and fast electron transfer properties (Qin et al., 2016). It can form thionine functionalized reduced graphene oxide (THI-rGO) nanocomposite by combining non-covalent synergistic charge transfer with rGO with excellent electrical conductivity and high specific surface area. And the positive charge on THI promotes solubility and prevents aggregation of rGO (Zhu et al., 2012). In brief, the well-dispersed THI-rGO was introduced as the substrate of sensor as well as signal generator. THI-rGO, gold nanoparticles (AuNPs), sDNA and 6-mercapto-1-hexanol (MCH) were successively modified on glassy carbon electrode (GCE, Φ = 3 mm). After that, fixing the ferrocene-labelled aptamer (Fc-apt) to the electrode by base pairing with sDNA. In this way, the regulation of current intensity ratio (I_{THI}/I_{Fc}) namely the ratiometric signal, can be achieved by changing modification of THI-rGO or the Fc-apt, and the resultant sensor presented the adjustable sensitivity. In the presence of AFB1, the formed Fc-apt-AFB1 complex released from the electrode surface, leading to the decrease of the impedance and the subsequent increase of I_{THI}. The ratiometric electrochemical biosensing platform with adjustable sensitivity could realize the accurate and reliable analysis of harmful substances in agricultural products, and may become a new universal platform for the development of versatile sensing in agricultural applications.

2. Experimental

2.1. Chemicals

Trisodium citrate ($Na_3C_6H_5O_7{\cdot}2H_2O$, ≥99.5 %, Sinopharm Chemical Reagent Co., Ltd), ethylenediaminetetraacetic acid disodium salt (EDTA, ≥99.0 %, Sinopharm Chemical Reagent Co., Ltd), tris hydroxymethyl aminomethan (Tris, 99.8 %, Alfa Aesar), thionine (THI, 100 %, Alfa Aesar), reduced graphene oxide (rGO, XFNANO Inc), aflatoxin B1 (AFB1, 98.0 %, Acros Organics), aflatoxin B2 (AFB2, 98.0 %, Acros Organics), fumonectin B1 (FB1, 96.0 %, Aladdin Chemistry) were employed in our work. The thiol-terminated AFB1 aptamer complementary chain, aptamer of AFB1 were synthesized by Sangon Biotech Co., Ltd (Shanghai, China), and the sequences were as follows (Castillo et al., 2015):

cDNA: 5′-*CGAGACACAGAGAGACA ACACGTGCCCAAC -$(CH_2)_6$-SH-3’*

Fc-apt: 5′-Fc-GTTGGGCACGTGTTGTCTCTCTGTGTCTCGTGCCCTTC GCTA

GGCCCACA-Fc-3′

DNA were dissolved in 10 mM Tris－HCl buffers (pH 7.4). And the prepared solution was stored at 4 °C as stock solution. All of purchased chemicals were utilized without further purification. Preparation of required solution by using ultrapure water.

2.2. Instrumentation

The morphology was demonstrated by transmission electron microscopy (TEM) on a JEM 1200EX TEM (JEOL, Japan). Scanning electron microscope (SEM) was recorded on a SU8020 SEM (Hitachi, Tokyo). X-ray photoelectron spectroscopy (XPS) analysis was recorded on ESCALAB250 (Thermo Fisher Scientific, USA). The UV–vis absorption spectrum was measured with a Lambda 750 UV–vis spectrophotometer (PerkinElmer, USA). Raman spectra was registered in LabRam HR (France). The electrochemical tests were conducted on a CHI 750E electrochemical workstation (Shanghai Chenhua, China). A traditional three-electrode system was used in our work. Different modified GCE were applied as the working electrode, and a platinum wire as the counter electrode and an Ag/AgCl (sat. KCl) electrode as the reference electrode. The electrochemical performance was investigated by alternating current voltammetry (ACV). And the ACV parameters adopted were as follows: a potential of 4 mV, a frequency of 25 Hz, and an amplitude of 25 mV by scanning the potential from -0.4 to 0.7 V in 100 mM PBS (pH 7.0). The assembly process of the aptasensor was investigated by the electrochemical impedance spectroscopy (EIS) in 0.1 M KCl containing 5 mM $Fe(CN)_6^{3-/4-}$ with a frequency range from 0.1 Hz to 100 kHz and 5 mV amplitude of sine voltage signal.

2.3. Preparations of THI-rGO

THI-rGO was synthesized according to the previous report with some modifications (Zhao et al., 2015). Briefly, rGO dispersion solution (15 mL, 0.1 mg mL^{-1}) was mixed with THI (3 mL, 10 μM) by magnetically stirring for 12 h. Then, the black dispersion was centrifuged (8000 rpm, 10 min) and washed with ultrapure water. And the resultant THI-rGO nanocomposite was dried and dispersed in 3 mL ultrapure water. Finally, the quantitative analysis of THI in THI-rGO composite was estimated with XPS and its concentration was calculated to be 0.141 mg mL^{-1}.

2.4. Preparation of ratiometric electrochemical aptasensor

Bare GCE was polished with 0.05 μm alumina powder, and then sonicated in ethanol and ultrapure water for 30 s to obtain a mirror surface. 6 μL of THI-rGO nanocomposite and AuNPs at a concentration of 5 nM were electrostatically adsorbed successively upon the surface of GCE and dry naturally at room temperature (Tao et al., 2019). After that, 6 μL cDNA was covalently anchored on the AuNPs via Au-S bond, and 6 μL of 1 mM MCH was used to block the nonspecific binding sites of AuNPs (Liang et al., 2014). Subsequently, Fc-apt was immobilized by the base pairing with cDNA. By regulating the modification of Fc-apt, the resultant aptasensor output different ratiometric signals. The aptasensor was stored at 4 °C before use.

2.5. Detection of AFB1

The standard AFB1 sample was prepared with 100 mM PBS (pH 7.0). 6 μL of AFB1 with certain concentration was casted on the aptasensor and incubated for 1 h, and then rinsed with 100 mM PBS (pH 7.0) before measurement.

2.6. Real sample pretreatment

For the preparation of samples, 20 *g* peanut (Zhenjiang, Jiangsu Province) was milled with 2 *g* of sodium chloride. A certain concentration of AFB1 was added to peanut flour (8 *g*), and then dissolved in 20 mL of extraction solvent ($V_{methanol}$:V_{water} = 6:4). After mixing for 60 min and centrifugation, the resultant extract was treated with 0.22 μm ultrafiltration membrane, followed by dilution with 100 mM PBS (pH 7.0) to a finally AFB1 concentration of 0.1 ng mL^{-1}, 1 ng mL^{-1}, 5 ng mL^{-1} and 10 ng mL^{-1}.

3. Results and discussion

3.1. Characterization of rGO, THI, THI-rGO, AuNPs

The morphology and structure of the prepared rGO (Fig. 1A) and THI-rGO (Fig. 1B) were characterized with SEM. The rGO displays the typical flake-like structure and wrinkles. For THI-rGO, the aggregation of THI can be observed on the rGO, in good agreement with previous report (Zhu et al., 2012). Based on the full scan XPS, the peaks at 532.6, 401.7 and 285.4 eV are associated with $O1_S$, $N1_S$ and $C1_S$, respectively, and the presence of $N1_S$ peak indicates the formation of THI-rGO (Fig. 1C) (Shahzad et al., 2017). Furthermore, the $N1_S$ spectrum is resolved into three peaks at 399.69 eV (C-N = C), 400.33 eV (C-NH_2), 402.67 eV (H-*N*-H), respectively, confirming the presence of THI in the synthesized composites (Fig. 1D).

UV-visible absorption spectrum was employed to monitor the formation of THI-rGO composite. The absorbances at 276 and 376 nm in the spectrum of rGO can be assigned to π-π* transitions of aromatic

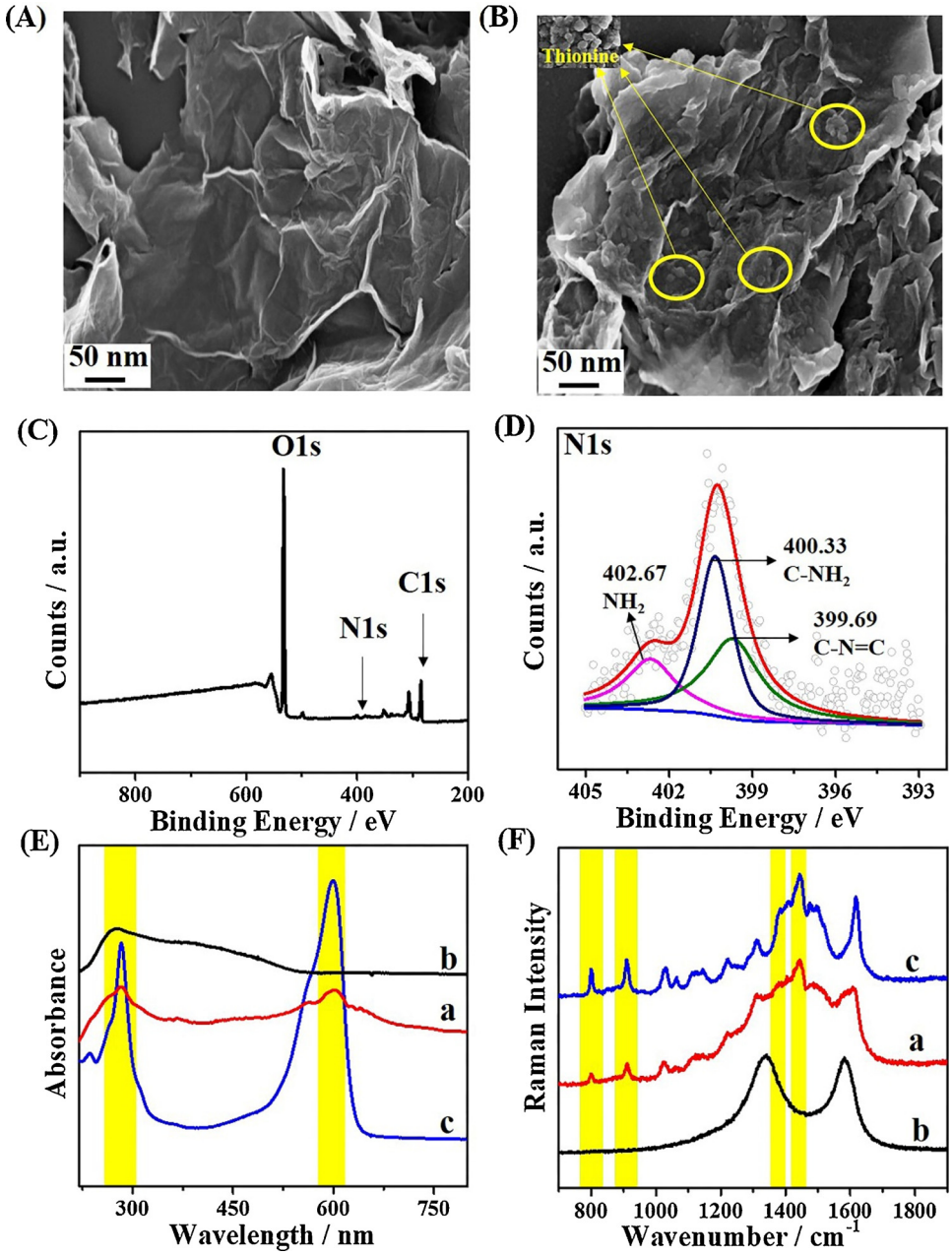

Fig. 1. SEM images of (A) rGO and (B)THI-rGO. (C) XPS spectra of THI-rGO. (D) Core-level XPS spectra of $N1_S$ of THI-rGO. (E) UV–vis absorption spectra of (a) rGO, (b) THI-rGO, (c) THI. (F) Raman spectra of (a) THI, (b) THI-rGO, and (c) rGO.

C=C bonds and n-π* transitions of −COOH, respectively (Fig. 1E, curve a). Three characteristic absorption peaks of THI are located at 283, 564 and 600 nm, corresponding to the π-π* transitions of aromatic rings, H-type dimer aggregate and n-π* transitions of C=N bond, respectively (Fig. 1E, curve c) (Zhu et al., 2012). All these absorption peaks observed in that of THI-rGO demonstrates the attachment of THI on rGO via π-π stacking (Fig. 1E, curve b) (Qin et al., 2016). Additionally, THI-rGO and THI display almost the same Raman spectra (Fig. 1F), indicating the negligible influence of interaction between THI and rGO on the native structure and properties of THI molecules (Li et al., 2004; Hao et al., 2018).

3.2. Characterization of electrochemical aptasensor

EIS measurements were performed in 0.1 M KCl solution containing 5 mM $[Fe(CN)_6]^{3-/4-}$ to monitor the aptasensor assembly (Fig. 2A), and fitted with the Randles equivalent circuit (Inset of Fig. 2A). The fitting parameters of the equivalent circuit were composed of the electrolyte solution (R_s), constant phase element (Q), electronic transfer resistance (R_{et}), and Warburg impedance (Z_w). Among them, the R_{et} value was estimated by the semicircle diameter of the EIS Nyquist curve, reflecting the electron transfer kinetics on the electrode interface. Compared with bare GCE (curve a), the modification of THI-rGO significantly reduces the R_{et} (42 Ω, curve b), suggesting its superior conductivity. The subsequent assembly of AuNPs leads to further decrease of R_{et} at the AuNPs/THI-rGO/GCE (curve c). Then, the successive assembly of cDNA, MCH and aptamer increase R_{et} to 540 Ω (curve d), 798 Ω (curve e), and 804 Ω (curve f), respectively, which are ascribed to the enlarged steric hindrance and electrostatic repulsion for $[Fe(CN)_6]^{3-/4-}$. After the addition of AFB1, a decrease of R_{et} is observed at AFB1/Fc-apt/MCH/cDNA/AuNPs/THI-rGO/GCE (647 Ω, curve g) owing to the stripping of Fc-aptamer-AFB1 complex from the electrode.

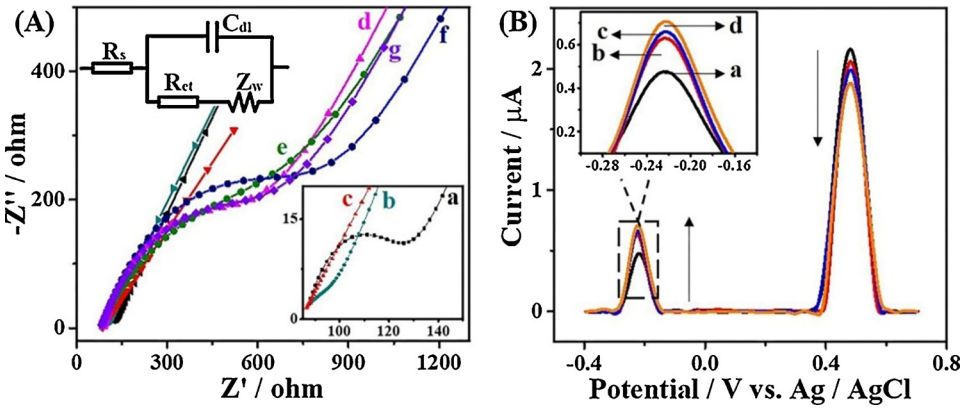

Fig. 2. (A) EIS operating in 0.1 M KCl aqueous solution containing 5 mM $[Fe(CN)_6]^{3-/4-}$ with the frequency varied from 0.1 Hz to 100 kHz and 5 mV amplitude of sine voltage signal. Nyquist plots of the electrode: (a) GCE, (b) THI-rGO/GCE, (c) AuNPs/THI-rGO/GCE, (d) cDNA/AuNPs/THI-rGO/GCE, (e) MCH/cDNA/AuNPs/THI-rGO/GCE, (f) Fc-apt/MCH/cDNA/AuNPs/THI-rGO/GCE, and (g) AFB1/Fc-apt/MCH/cDNA/AuNPs/THI-rGO/GCE. Inset: Equivalent circuit corresponding to the impedance features of the modified electrode. The equivalent circuit used to fit the EIS Nyquist plots in this work consisted of the resistance of the electrolyte solution (R_s), constant phase element (Q), electron transfer resistance (R_{et}), and Warburg impedance (Z_w). (B) ACV responses toward AFB1 with the concentration of (a) 0.0 ng mL^{-1}, (b) 1.0 ng mL^{-1}, (c) 10 ng mL^{-1}, (d) 100 ng mL^{-1} in 100 mM PBS (pH 7.0), and magnified view of THI signal at 0.2 V.

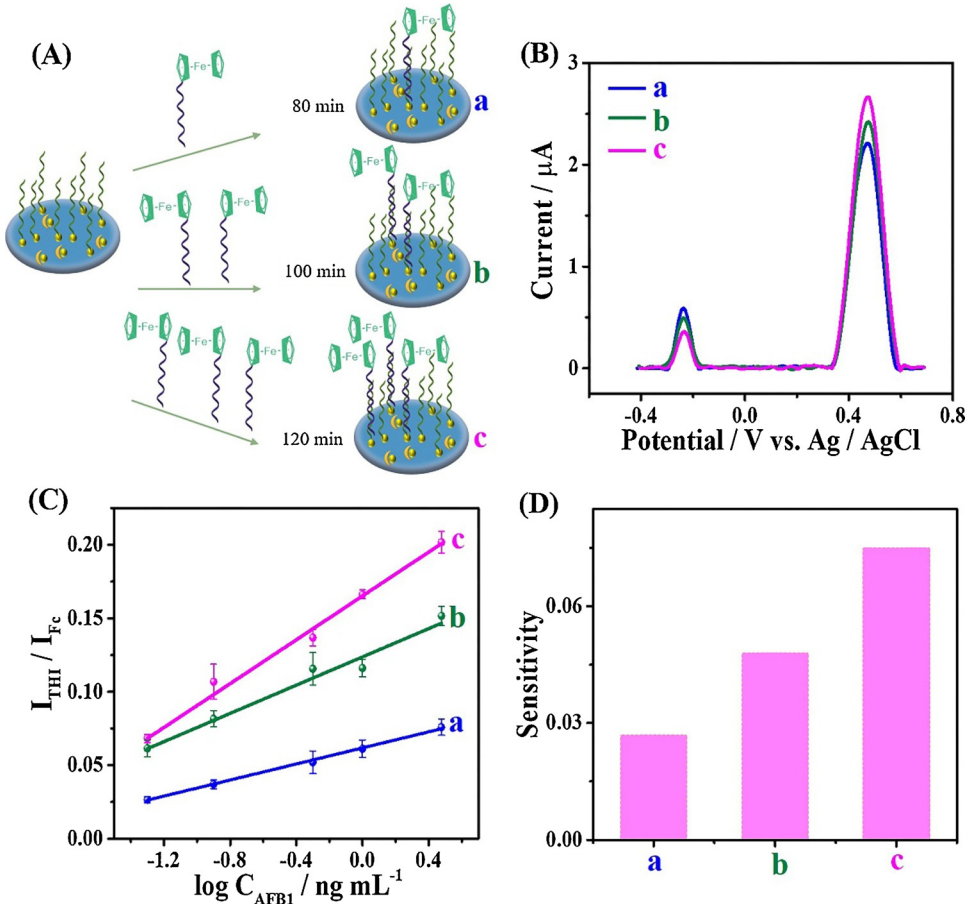

Fig. 3. (A) The illustration of the fabrication of three aptasensors with different ratiometric signals by differing the incubation time of Fc-apt with 80 min (a), 100 min (b), 120 min (c). (B) ACV responses at the resultant aptasensors. (C) Logarithmic dependence of the ACV peak current ratiometric of I_{THI}/I_{Fc} with the different concentration of AFB1: 0.05 ng mL^{-1}, 0.12 ng mL^{-1}, 0.5 ng mL^{-1}, 1 ng mL^{-1}, 3 ng mL^{-1}. (D) Relationship between I_{THI}/I_{Fc} and sensitivity.

These results indicate the successful fabrication of electrochemical sensing interface for AFB1.

3.3. Feasibility of the electrochemical aptasensor for AFB1 assay

ACV measurements were conducted to evaluate the feasibility of the proposed aptasensor for AFB1. As shown in Fig. 2B, two peaks at 0.2 V and 0.48 V are observed at Fc-apt/MCH/cDNA/AuNPs/THI-rGO/GCE, which are assigned to the oxidation of THI and Fc, respectively (curve a). After the addition of 1 ng mL^{-1} AFB1, the current intensities of Fc (I_{Fc}) and THI (I_{THI}) decreases and increases, respectively, resulting from the stripping of the Fc-aptamer-AFB1 complex (curve b). With increasing the concentration of AFB1 (C_{AFB1}), the change of I_{Fc} and I_{THI} exhibits the same trend, and thus the I_{THI}/I_{Fc} could be used as the signal for AFB1 detection, indicating the feasible of the proposed strategy for AFB1 sensing.

We then optimized the experimental conditions including aptamer incubation time, concentration, and target incubation time, which are provided in supporting information (Fig. S2).

3.4. Sensitivity analysis of aptasensor detection of AFB1

The testing demands for AFB1 analysis in agricultural products (e.g. peanut) differs in periods such as planting, transportation, storage and processing (Casada and Young, 1994; Luo et al., 2019; Passone et al., 2010; Lavkor and Var, 2017). Herein, we envisaged to regulate the ratiometric signal by tuning the assembly of Fc-apt to achieve programmable sensitivity of aptasensor. As shown in Fig. 3A, three

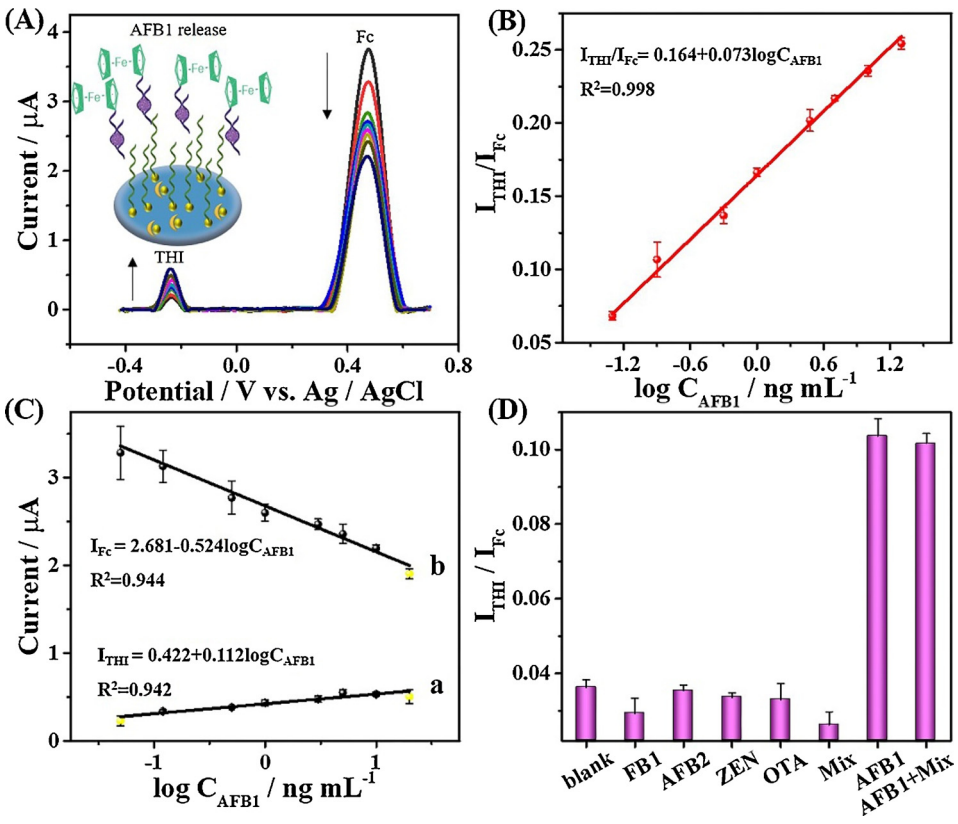

Fig. 4. (A) ACV responses for AFB1 with different concentrations (0.05, 0.12, 0.5, 1, 3, 5, 10, 20 ng mL^{-1}); Solution: 100 mM PBS (pH 7.0). (B) The calibration curve for AFB1 determination (plot of I_{THI}/I_{Fc} vs. logarithm of the AFB1 concentration (C_{AFB1})). (C) Logarithmic dependence of C_{AFB1} on (a) I_{THI} and (b) I_{Fc}. (D) Comparison of the responses to 0.5 ng mL^{-1} solution of AFB1 and 10 ng mL^{-1} solution of FB1, AFB2, ZEN, OTA and the mixture of the interferences at the aptasensor.

Table 1
Comparisons of the proposed method with the reported methods for AFB1 detection.

Methods	Linear ranges (ng mL^{-1})	Detection limits (ng mL^{-1})	Refs.
EC	0.125-16	0.12	Castillo et al. (2015)
EC	30-3000	10	Zhang et al. (2016)
EC	0.05-6.0	0.05	Goud et al. (2017)
EC	–	0.017	Evtugyn et al. (2014)
Colorimetric	0.1-10000	0.1	Seok et al. (2015)
RS	–	0.1	Ko et al. (2015b)
MZIs	–	0.8	Pagkali et al. (2018)
FL	5–100	1.6	Chen et al. (2017)
CL	0.1–10	0.11	Shim et al. (2014)
REC	**0.05–20**	**0.016**	**Our work**

Abbreviations: RS-Raman scattering; FL-Fluorescence; CL-Chemiluminescence; REC-Ratiometric electrochemistry; MZIs-Mach-Zehnder interferometers.

aptasensors were prepared simply by differing the incubation time of Fc-apt, presenting the I_{THI}/I_{Fc} values of 0.26 (a), 0.20 (b) and 0.14 (c), and their ACV curves are shown in Fig. 3B. As a proof of concept, these aptasensors were applied to the AFB1 analysis with concentrations ranging from 0.05 to 3 ng mL^{-1}, and the corresponding calibration curves are shown in Fig. 3C. Consequently, the calculated sensitivity of aptasensor a, b and c are 0.027, 0.048, and 0.076, respectively, confirming the feasibility of sensitivity adjustment by the regulation of ratiometric signal (Fig. 3D). The aptasensor c displayed the highest sensitivity, and it was employed for the following experiments.

3.5. Determination of AFB1 by ACV

The detailed analytical performances of aptasensor c were evaluated by monitoring the change of I_{THI}/I_{Fc} toward different C_{AFB1}. As shown in Fig. 4A, the increases of I_{THI} and the decreases of I_{Fc} are observed with the raising of C_{AFB1}. On the logarithmic scale, the I_{THI}/I_{Fc} value is linearly related to C_{AFB1} from 0.05 to 20 ng mL^{-1} and a detection limit (LOD) down to 0.016 ng mL^{-1} (defined as S/N = 3) (Fig. 4B). The corresponding regression equation is I_{THI}/I_{Fc} = 0.073 logC_{AFB1} + 0.164 with a correlation coefficient (R^2) of 0.998. The analytical properties of the aptasensor based on the individual signal I_{THI} or I_{Fc} were also investigated. As shown in Fig. 4C, both I_{THI} and I_{Fc} exhibit linear variation with C_{AFB1} ranging from 0.1 to 10 ng mL^{-1}, presenting a relatively low R^2 of 0.941 and poor LOD of 0.033 ng mL^{-1}. Thus, the proposed ratiometric strategy could effectively improve both sensitivity and accuracy for AFB1 analysis.

Compared with the previously reported assays for AFB1 including

Table 2
Comparison of results by the proposed method and HPLC-FL for AFB1 analysis in peanut (n = 3).

Sample	Spiked (ng mL^{-1})	Proposed method (n = 3)			HPLC-FL	
		Detected (ng mL^{-1})	RSD (%)	Recovery (%)	Detected (ng mL^{-1})	Recovery (%)
1	0	–	–	–	–	–
2	0.1	0.0865	2.5	86.5	0.123	123
3	1	1.11	6.0	111	1.11	111
4	5	5.60	6.6	112	4.98	99.6

electrochemistry (EC) (Castillo et al., 2015; Zhang et al., 2016; Goud et al., 2017; Evtugyn et al., 2014), colorimetric (Seok et al., 2015), Raman scattering (RS) (Ko et al., 2015b), optical method (Pagkali et al., 2018), fluorescence (FL) (Chen et al., 2017) and chemiluminescence (CL) (Shim et al., 2014), the proposed ratiometric electrochemical aptasensor exhibits a large dynamic range and low LOD (Table 1).

3.6. Selectivity, reproducibility and stability of ratiometric electrochemical aptasensor

The selectivity of the proposed aptasensor was evaluated by using common mycotoxins including FB1, AFB2, ZEN, OTA as interferents. As showed in Fig. 4D, in the presence of FB1 (10 ng mL^{-1}), AFB2 (10 ng mL^{-1}), ZEN (10 ng mL^{-1}) or OTA (10 ng mL^{-1}), almost the same I_{THI}/I_{Fc} value are obtained at the proposed aptasensor as that of the blank test. However, significantly increased of I_{THI}/I_{Fc} value is observed upon the addition of 0.5 ng mL^{-1} AFB1 or the mixture of AFB1 (0.5 ng mL^{-1}) and the above-mentioned disturbances (10 ng mL^{-1}). These results suggest the superior selectivity of proposed aptasensor toward the detection of AFB1.

The reproducibility and stability of the proposed aptasensor were estimated by monitoring 0.12 ng mL^{-1} of AFB1 (Fig. S3). The aptasensor have higher reproducibility by measuring six batches of aptasensors, and the relative standard deviation (RSD) of 1.79 % indicates the satisfactory reproducibility (Fig. S3A). The stability of the aptasensor was studied by measuring the ACV signal for different time periods. After 7 days of storage, the peak current showed the neglectable change. And the RSD of peak currents was calculated to be 2.25 % (n = 6), suggesting the superior stability of aptasensor (Fig. S3B).

3.7. Analysis of AFB1 in spiked peanut samples

To explore the analytical performance for real samples, the aptasensor was used for the detection of AFB1 in peanut. The samples were prepared by dissolving, centrifuging and filtering. As shown in Table 2, the recoveries of spiked samples range from 86.5%–112.0% with RSD below 6.6 %, which are acceptable for practical detection. The accuracy of proposed method was verified with the national standard method of high-performance liquid chromatography-fluorescence (HPLC-FL). As shown in Table 2, both of these two methods display the satisfactory recoveries, suggesting the comparable accuracy of the proposed method for real sample analysis.

4. Conclusion

In summary, a novel sensitivity programmable ratiometric electrochemical aptasensor for AFB1 analysis on the basis of ratiometric signal regulation was constructed. The relationship between the sensitivity of the aptasensor and the value of ratiometric signal was illustrated, and the programmable sensitivity was achieved by tuning the assembly of Fc-apt. Following this principle, the proof-of-concept ratiometric electrochemical aptasensors with different sensitivities were successfully fabricated, and the aptasensor with the highest sensitivity showed wide linear range and relatively low LOD with superior reproductivity and stability toward AFB1 analysis. In addition, such a sensing platform displayed the satisfactory applicability for the analysis of peanut sample. More importantly, the proposed ratiometric electrochemical aptasensor is versatile to survey other mycotoxins in the field of agriculture interactions by simply replacing the corresponding DNA.

CRediT authorship contribution statement

Yuye Li: Investigation, Data curation, Writing - original draft. **Dong Liu:** Methodology, Conceptualization, Formal analysis, Writing - review & editing. **Chengxi Zhu:** Resources, Software. **Xiuli Shen:** Resources, Software. **Yang Liu:** Writing - review & editing. **Tianyan You:** Supervision, Conceptualization, Writing - review & editing.

Declaration of Competing Interest

We declare that we have no financial and personal relationships with other people or organizations that can inappropriately influence our work, there is no professional or other personal interest of any nature or kind in any product, service and/or company that could be construed as influencing the position presented in, or the review of, the manuscript entitled.

Acknowledgments

This work was supported by National Natural Science Foundation of China (No. 21675065, 61901193), Natural Science Foundation of Jiangsu Province (No. BK20160490), the Innovation/Entrepreneurship Program of Jiangsu Province, Priority Academic Program Development of Jiangsu Higher Education Institutions.

Appendix A. Supplementary data

Supplementary material related to this article can be found, in the online version, at doi:https://doi.org/10.1016/j.jhazmat.2019.122001.

References

Amaya-González, S., López-López, L., Miranda-Castro, R., de-los-Santos-Álvarez, N., Miranda-Ordieres, A.J., Lobo-Castañón, M.J., 2015. Affinity of aptamers binding 33-mer gliadin peptide and gluten proteins: influence of immobilization and labeling tags. Anal. Chimi. Acta 873, 63–70.

Babu, D., Muriana, P.M., 2011. Immunomagnetic bead-based recovery and real time quantitative PCR (RT iq-PCR) for sensitive quantification of aflatoxin B1. J. Microbiol. Meth. 86, 188–194.

Bizzotto, D., Burgess, I.J., Doneux, T., Sagara, T., Yu, H.Z., 2018. Beyond simple cartoons: challenges in characterizing electrochemical biosensor interfaces. ACS Sens. 3, 5–12.

Capriotti, A.L., Cavaliere, C., Foglia, P., Samperi, R., Stampachiacchiere, S., Ventura, S., Laganà, A., 2014. Multiclass analysis of mycotoxins in biscuits by high performance liquid chromatography tandem mass spectrometry. Comparison of different extraction procedures. J. Chromatogr. A 1343, 69–78.

Casada, M.E., Young, J.H., 1994. Heat and moisture transfer during transportation of shelled peanuts. Am. J. Agrc. Econ. 37, 1939–1946.

Castillo, G., Spinella, K., Poturnayová, A., Šnejdárková, M., Mosiello, L., Hianik, T., 2015. Detection of aflatoxin B1 by aptamer based biosensor using PAMAM dendrimers as immobilization platform. Food Control 52, 9–18.

Chen, L., Wen, F., Li, M., Guo, X.D., Li, S.L., Zheng, N., Wang, J.Q., 2017. A simple aptamer based fluorescent assay for the detection of aflatoxin B1 in infant rice cereal. Food Chem. 215, 377–382.

Crisan, E.V., 1973. Effects of aflatoxin on seedling growth and ultrastructure in plants. Appl. Environ. Microbiol. 26, 991–1000.

Daradimos, E., Marcaki, P., Koupparis, M., 2000. Evaluation and validation of two fluorometric HPLC methods for the determination of aflatoxin B1 in olive oil. Food Addit. Contam. 17, 65–73.

Ediage, E.N., Di Mavungu, J.D., Monbaliu, S., Van Peteghem, C., De Saeger, S., 2011. A validated multianalyte LC-MS/MS method for quantification of 25 mycotoxins in cassava flour, peanut cake and maize samples. J. Agric. Food Chem. 59, 5173–5180.

Evtugyn, G., Porfireva, A., Stepanova, V., Sitdikov, R., Stoikov, I., Nikolelis, D., Hianik, T., 2014. Electrochemical aptasensor based on polycarboxylic macrocycle modified with neutral red foraflatoxin B1 detection. Electroanalysis 26, 2100–2109.

Goodman, L.S., 1996. Goodman and Gilman's the Pharmacological Basis of Therapeutics. McGraw-Hill, New York.

Goud, K.Y., Hayat, A., Catanante, G., S. M, Gobi, K.V., Marty, J.L., 2017. An electrochemical aptasensor based on functionalized graphene oxide assisted electrocatalytic signal amplification of methylene blue for aflatoxin B1 detection. Electrochim. Acta 244, 96–103.

Hao, N., Hua, R., Chen, S., Zhang, Y., Zhou, Z., Qian, J., Liu, Q., Wang, K., 2018. Multiple signal-amplification via Ag and TiO_2 decorated 3D nitrogen doped graphene hydrogel for fabricating sensitive label-free photoelectrochemical thrombin aptasensor. Biosens. Bioelectron. 101, 14–20.

Jeong, J.E., Kim, B., Lee, J., Kyhm, K., Woo, H.Y., 2017. Inhibitor effects on molecular beacon-based mercury assays for tuning of detection range. Sen. Actuators B: Chem. 240, 810–817.

Karapetis, S., Nikolelis, D., Hianik, T., 2018. Label-free and redox markers-based electrochemical aptasensors for aflatoxin M1 detection. Sensors 18, 4218.

Kékedy-Nagy, Ls., Ferapontova, E.E., 2018. Sequence-specific electron transfer mediated by DNA duplexes attached to gold through the alkanethiol linker. J. Phys. Chem. B 122, 10077–10085.

Ko, J., Lee, C., Choo, J., 2015a. Highly sensitive SERS-based immunoassay of aflatoxin B1 using silica-encapsulated hollow gold nanoparticles. J. Hazard. Mater. 285, 11–17.

Ko, J., Lee, C., Choo, J., 2015b. Highly sensitive SERS-based immunoassay of aflatoxin B1 using silica encapsulated hollow gold nanoparticles. J. Hazard. Mater. 285, 11–17.
Lavkor, I., Var, I., 2017. The Control of Aflatoxin Contamination at Harvest, Drying, Pre-storage and Storage Periods in Peanut: the New Approach, Aflatoxin-control, Analysis, Detection and Health Risks.
Li, Y., Chang, Y., Ma, J., Wu, Z., Yuan, R., Chai, Y., 2019. Programming a target-initiated bifunctional DNAzyme nanodevice for sensitive ratiometric electrochemical biosensing. Anal. Chem. 91, 6127–6133.
Li, Q.W., Zhang, J., Yan, H., He, M.H., Liu, Z.F., 2004. Thionine mediated chemistry of carbon nanotubes. Carbon 42, 287–291.
Liang, R.P., Tian, X.C., Qiu, P., Qiu, J.D., 2014. Multiplexed electrochemical detection of trypsin and chymotrypsin based on distinguishable signal nanoprobes. Anal. Chem. 86, 9256–9263.
Liu, J., Sun, L., Zhang, J., Guo, J., Chen, L., Qi, D., Zhang, N., 2016. Aflatoxin B1, zearalenone and deoxynivalenol in feed ingredients and complete feed from central China. Food Addit. Contam. Part B Surveill. 9, 91–97.
Luo, L.J., Ma, S., Li, L.B., Liu, X.H., Zhang, J.Y., Li, X., Liu, D., You, T.Y., 2019. Monitoring zearalenone in corn flour utilizing novel self-enhanced electrochemiluminescence aptasensor based on NGQDs-NH_2-Ru@SiO_2 luminophore. Food Chem. 292, 98–105.
Pagkali, V., Petrou, P.S., Makarona, E., Peters, J., Haasnoot, W., Jobst, G., Moser, I., Gajos, K., Budkowski, A., Economou, A., Misiakos, K., Raptis, I., Kakabakos, S.E., 2018. Simultaneous determination of aflatoxin B1, fumonisin B1 and deoxynivalenol in beer samples with a label-free monolithically integrated optoelectronic biosensor. J. Hazard. Mater. 359, 445–453.
Passone, M.A., Rosso, L.C., Ciancio, A., Etcheverry, M., 2010. Detection and quantification of aspergillus section flavi spp. in stored peanuts by real time PCR of nor-1 gene, and effects of storage conditions on aflatoxin production. J. Food Microbiol. Saf. Hyg. 138, 276–281.
Qin, X.L., Yin, Y., Yu, H.J., Guo, W.J., Pei, M.S., 2016. A novel signal amplification strategy of an electrochemical aptasensor for kanamycin, based on thionine functionalized graphene and hierarchical nanoporous PtCu. Biosens. Bioelectron. 77, 752–758.
Seok, Y., Byun, J.Y., Shim, W.B., Kim, M.G., 2015. A structure switchable aptasensor for aflatoxin B1 detection based on assembly of an aptamer/split DNAzyme. Anal. Chim. Acta 886, 182–187.
Shahzad, F., Zaidi, S.A., Koo, C.M., 2017. Highly sensitive electrochemical sensor based on environmentally friendly biomass derived sulfur doped graphene for cancer biomarker detection. Sen. Actuators B: Chem. 241, 716–724.
Shim, W.B., Mun, H., Joung, H.A., Ofori, J.A., Chung, D.H., Kim, M.G., 2014. Chemiluminescence competitive aptamer assay for the detection of aflatoxin B1 in corn samples. Food Control 36, 30–35.
Shimizu, H., Miyawaki, N., Asano, Y., Mawatari, K., Kitamori, T., 2017. Thermo-optical characterization of photothermal optical phase shift detection in extended-nano channels and UV detection of biomolecules. Anal. Chem. 89, 6043–6049.
Tao, D., Shui, B., Gu, Y., Cheng, J., Zhang, W., Jaffrezic-Renault, N., Song, S., Guo, Z., 2019. Development of a label-free electrochemical aptasensor for the detection of tau381 and its preliminary application in AD and non-AD patients' sera. Biosens. 9, 84.
Wang, X., Que, M., Chen, M., Han, X., Li, X., Pan, C., Wang, Z.L., 2017. Sensors: full dynamic-range pressure sensor matrix based on optical and electrical dual-mode sensing. Adv. Mater. 29, 1605817.
WHO, 1993. IARC Monographs on the Evaluation of Carcinogenic Risk to Humans, Vol. 56, Some Naturally Occurring Substances: Food Items and Constituents, Heterocyclic Aromatic Amines and Mycotoxins. WHO.
Wu, L., Ding, F., Yin, W., Ma, J., Wang, B., Nie, A., Han, H., 2017. From electrochemistry to electroluminescence: development and application in a ratiometric aptasensor for aflatoxin B1. Anal. Chem. 89, 7578–7585.
Yang, T., Yu, R., Yan, Y., Zeng, H., Luo, S., Liu, N., Morrin, A., Luo, X., Li, W., 2018. A review of ratiometric electrochemical sensors: from design schemes to future prospects. Sen. Actuators B: Chem. 274, 501–516.
Zhang, H., Jia, S., Lv, M., Shi, J., Zuo, X., Su, S., Wang, L., Huang, W., Fan, C., Huang, Q., 2014. Size-dependent programming of the dynamic range of graphene oxide DNA interaction-based ion sensors. Anal. Chem. 86, 4047–4051.
Zhang, X., Li, C.R., Wang, W.C., Xue, J., Huang, Y.L., Yang, X.X., Tan, B., Zhou, X.P., Shao, C., Ding, S.J., Qiu, J.F., 2016. A novel electrochemical immunosensor for highly sensitive detection of aflatoxin B1 in corn using single-walled carbon nanotubes/chitosan. Food Chem. 192, 197–202.
Zhao, Z., Chen, H.D., Ma, L.N., Liu, D.J., Wang, Z.X., 2015. A label free electrochemical impedance aptasensor for cylindrospermopsin detection based on thionine-graphene nanocomposites. Analyst 140, 5570–5577.
Zhu, C.X., Liu, D., Li, Y.Y., Shen, X.L., Li, L.B., Liu, Y., You, T.Y., 2019. Ratiometric electrochemical, electrochemiluminescent and photoelectrochemical strategies for environmental contaminant detection. Curr. Opin. Electrochem. 17, 47–55.
Zhu, L.M., Luo, L.Q., Wang, Z.X., 2012. DNA electrochemical biosensor based on thionine-graphene nanocomposite. Biosens. Bioelectron. 35, 507–511.
Zhuang, Z., Huang, Y., Yang, Y., Wang, S., 2016. Identification of AFB1-interacting proteins and interactions between RPSA and AFB1. J. Hazard. Mater. 301, 297–303.